RSC Advances

PAPER

View Article Online
View Journal | View Issue

Cite this: *RSC Adv.*, 2023, **13**, 5219

Thermal degradation and flame retardancy of nylon 6/aluminum methylmethoxy phosphonate composites†

Hai Vothi, *[abc] Chowon Kim,[d] TanBinh Nguyen,[d] Jinwoo Lee,[d] Lan-Anh T. Nguyen[e] and Jonghwan Suhr*[df]

An aluminum methylmethoxyphosphonate (AlPo)-based flame retardant (FR) was synthesized. Thermal degradation and flame retardancy of nylon 6 (PA6)/AlPo composites were examined and compared with PA6/commercial aluminum diethylphosphinate (AlPi) composites. The PA6/AlPo composite achieved a V-0 rating at 20 wt% loading during the UL-94 test, and it exhibited the formation of a charred layer that protected the polymer from burning and reduced the release of gases during the combustion of PA6. AlPo demonstrated exceptional performance in gaseous and condensed phases in the PA6 matrix, whereas AlPi only worked in the gaseous phase. The differences between the thermal degradation mechanisms and flame retardancies of AlPi and AlPo were investigated *via* Fourier-transform infrared (FT-IR) spectroscopy, thermogravimetric analysis (TGA), scanning electron microscopy (SEM), and cone calorimetry. A suitable degradation mechanism was proposed to aid the development of flame retardants in the future.

Received 16th November 2022
Accepted 6th February 2023

DOI: 10.1039/d2ra07297a

rsc.li/rsc-advances

1. Introduction

Recently, the demand for environment-friendly electric vehicles has significantly increased. This has led to an increase in the production of electric batteries that are crucial components in electric and hybrid vehicles.[1–4] Therefore, the demand for polymers that can be used for high-temperature applications, particularly for electrical and electronics applications, has rapidly increased. The battery housing cover is a critical component, and it should have high flame retardancy to prevent accidents. Polyamide 6 (PA6) is a typical material that is widely used as an engineering plastic in electronic and electrical, telecommunication, and traffic devices due to its exceptional mechanical strength, abrasion resistance, electrical insulation and thermal properties.[5–7] However, intrinsic flammability and poor flame retardancy are the drawbacks of neat PA6. Therefore, a flame retardant (FR) with high efficiency and thermal stability is required for PA6 structures.[8–10]

Organo-phosphorus FRs based on aliphatic structures with higher phosphorous content than in aromatic structures have low thermal stability and decompose at relatively lower temperatures and/or become water soluble. These drawbacks are critical while developing an organo-phosphorus FR for PA6, which decomposes at significantly high temperatures.[11–15] High P content can be obtained without losing the thermal and hydroscopic stabilities by converting a simple phosphorus acid into a salt by complexing with a metal atom. For example, phosphinic or phosphonic acids are complexed with aluminum atoms, and the resulting aluminum phosphinate or phosphonate, respectively, becomes thermally stable and water-insoluble.[16–18]

The aluminum salt of diethyl phosphinate (AlPi) is a highly effective phosphorus-based flame retardant (FR) for materials such as PA6 due to its high thermal stability and good flame retardancy in gaseous phase.[19–21] PA6T can obtain V-0 rating in UL-94 tests using 17.5 wt% OP1230-based AlPi loading.[22] However, AlPi releases large amounts of heat and smoke during combustion due to the gaseous phase mechanism. A similar tendency is observed for various organo-phosphorus-based FRs.[23] Polymers such as PA6 do not exhibit charring. They exhibit random scission degradation, which is unsuitable with FRs that generate excessive char.

This study aimed to determine a suitable FR that can effectively function as a fire retardant in the gaseous phase to decrease fire hazards of the material, form char in the

[a]*Center for Composite Materials & Concurrent Design, Research & Business Foundation, Sungkyunkwan University, Suwon, 16419, Republic of Korea. E-mail: vthai@hcmus.edu.vn; Tel: +84339949314*
[b]*University of Science, Ho Chi Minh City, Vietnam*
[c]*Vietnam National University Ho Chi Minh City, Vietnam*
[d]*Department of Polymer Science and Engineering, Sungkyunkwan University, Suwon, 16419, Republic of Korea. E-mail: suhr@skku.edu; Tel: +821077087847*
[e]*Department of Energy Science, Sungkyunkwan University, Suwon, 16419, Republic of Korea*
[f]*Department of Mechanical Engineering, Sungkyunkwan University, Suwon, 16419, Republic of Korea*

† Electronic supplementary information (ESI) available. See DOI: https://doi.org/10.1039/d2ra07297a

condensed phase to protect the polymer from burning, and reduce the generation of heat and release of gases during combustion. Organo-phosphonate-based aluminum methylmethoxyphosphonate (AlPo) was selected as a potential FR to replace AlPi to ensure effective FR performance and minimize the amount of heat and gas generated during combustion. AlPo was synthesized and used as a FR for GF-PBT.[17] However, it has not been studied on PA6. Herein, AlPo was synthesized under simple conditions with higher yield and applied to PA6. The thermal decomposition mechanism of AlPo in PA6 was investigated in detail to determine the flame retardancy in gaseous and condensed phases that occur in PA6. This process was performed and compared with that of AlPi-based commercial Exolit OP1230 from Clariant Company.

2. Experiments

2.1 Materials

Polyamide 6 pallets (nylon 6, PA6) were provided by Taekwang Company, Korea. AlPi Exolit OP1230 was purchased from Clariant. Dimethyl methyl phosphonate (DMMP) and aluminum sulfate monohydrate (ASH) were purchased from Sigma-Aldrich. Sodium hydroxide was purchased from Samchun Company, Korea.

2.2 Synthesis of aluminum methylmethoxyphosphonate (AlPo)

AlPo was synthesized *via* two steps as shown in Fig. 1. First, 124 g of DMMP (1 mol) was added in 500 mL distilled water and placed into 2 L Erlene equipped with a magnetic stirring bar and heater. Subsequently, 40 g of sodium hydroxide (1 mol) was dissolved in 500 mL distilled water and slowly dropped into Erlene at room temperature. Thereafter, the solution was allowed to react for 6 h at room temperature. In the second step, 51.3 g of aluminum sulfate hydrate (0.15 mol) was dissolved in 500 mL distilled water and added into Erlene at room temperature. The solution was heated to 70 °C and was allowed to react for least 5 days. The AlPo product was filtered and washed thrice with distilled water to eliminate by-products, and it was dried overnight under vacuum at 60 °C. The success of the synthesized AlPo was determined and evaluated using FT-IR, SEM-energy dispersive spectrometry (EDS), and TGA analyses.

2.3 Preparation of PA6/AlPi and PA6/AlPo composites

PA6 was dried at 60 °C under vacuum condition for 5 h to eliminate water adsorption before compounding. The mixture of PA6 with the FR at the designated composition was blended in a Haake PolyDrive mixer at 230 °C for 7 min at 60 rpm. Subsequently, the mixture was hot-pressed at 230 °C under 10 MPa for 5 min into sheets that were cut into suitably sized specimens for the fire test.

2.4 Measurements

The thermogravimetric analysis (TGA) and differential thermal analysis (DTA) were performed using a TG/DTA7300 thermal analyzer (EXSTAR). The samples were heated from 35 °C to 700 °C at a heating rate of 10 °C min^{-1} under nitrogen or air conditions. Each sample was examined twice to confirm the reproducibility where the acceptable difference between the two runs was <2 wt%.

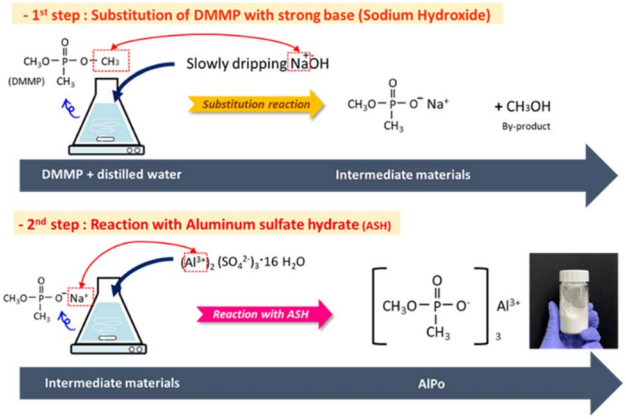

Fig. 1 Synthesis scheme of aluminum methylmethoxyphosphonate (AlPo).

Fourier-transform infrared (FT-IR) spectra were recorded using a BRUKER-IFS-66/S, TENSOR 27 spectrometer using KBr pellets. The transition mode was used, and the wavenumber range was set as 4000–400 cm^{-1}.

Micromorphology of the char residues was observed using field-emission scanning electron microscopy (SE-SEM) (JSM-7600F instrument) at an acceleration voltage of 10 kV. The EDS provided a chemical analysis of FRs that were conducted on a JSM-7600F SEM instrument at an acceleration voltage of 10 kV. A coating of platinum was applied on the surface of the samples for SEM observation.

UL-94 vertical burning test was evaluated according to the testing procedure of ASTM D3801 with a specimen size of 130 × 13.0 × 3.2 mm^3 (length × width × thickness). The fire retardancies of the samples were evaluated according to the following protocol. The test specimen rod was placed in a holder in the vertical position and the lower end of the rod was brought in contact with a butane flame for 10 s to initiate burning, and subsequently, the flame was removed. The time until the flaming stopped was measured. The flame was reapplied for additional 10 s and then removed. The time until the flaming stopped was measured again. Two sets of five specimens were evaluated. Three UL-94 ratings were considered (V-0, V-1, and V-2) depending upon the average flaming time after the first/second ignitions and the occurrence of drips as shown below.

- V-0: burning stops within 10 s and no drips allowed.
- V-1: burning stops within 30 s and no drips allowed.
- V-2: burning stops within 30 s and drips of faming particles are allowed.

The combustion behavior was measured using a cone calorimeter device (Dual Cone Calorimeter, Fire Testing Technology, East Grinstein, UK) exposing a radiant cone at a heat flux of 50 kW m^{-2} according to ISO5660-1 and the size of the

samples was 100.0 × 100.0 × 3.0 mm^3 (length × width × thickness).

3. Results and discussion

3.1 Characterization of FRs

The chemical structures of AlPi and the synthesized AlPo were spectroscopically analyzed using FT-IR and are shown in Fig. 2. According to the FT-IR spectrum line of AlPi, three strong absorption peaks of AlPi were obtained at wavenumbers of 1076 cm^{-1} (stretching vibration of P–O), 1152 cm^{-1} (P═O vibration), and 780 cm^{-1} (P–C vibration) along with the typical absorption peaks at 2780 and 2962 cm^{-1} related to C–H stretching vibrations. This result was identified and it corresponded to the structure of OP1230.[24] In comparison, the FT-IR spectrum of synthesized AlPo exhibited three typical strong peaks corresponding to P–O, P═O, and P–C at wavenumbers of 1044, 1168, and 806 cm^{-1}, respectively. In addition, the stretching vibrations of C–H bonding were observed at wavenumbers of 2854 and 2951 cm^{-1}. Moreover, the spectrum line of AlPo exhibited two strong adsorption peaks that were absent in the spectrum line of AlPi for CH_3–P and P–O–C bonds at wavenumbers 1103 and 903 cm^{-1}, respectively. Moreover, the obtained white-solid AlPo is insoluble in water and the FT-IR result of AlPo has been verified in advance in literature.[17] The above obtained values proved that AlPo was successfully synthesized using the proposed method.

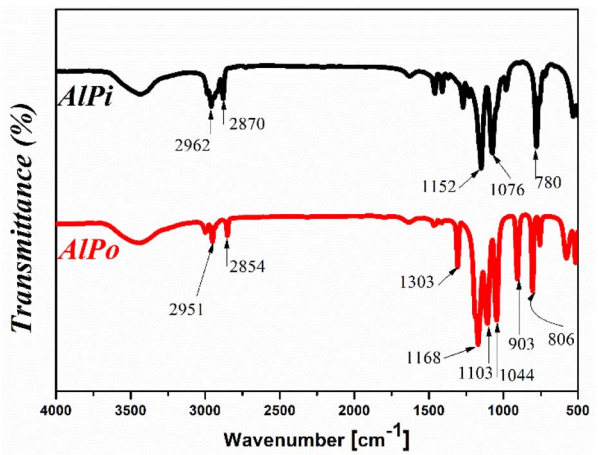

Fig. 2 FT-IR spectra of AlPi and synthesized AlPo.

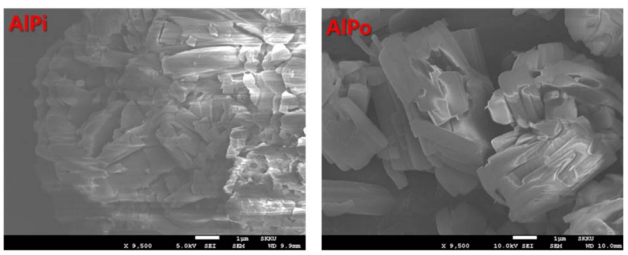

Fig. 3 SEM micrograph of AlPi and synthesized AlPo.

For further investigation, the surface morphology information of AlPi and synthesized AlPo was examined using SEM and EDS analyses as shown in Fig. 3. It can be observed that the SEM images of AlPi and synthesized AlPo exhibited micro rod-shaped particles and a similar agglomeration phenomenon was observed. Additional EDS information provided in ESI S1† shows that AlPi and synthesized AlPo were composed of Al, C, O, H, and P elements. Therefore, FT-IR and SEM with EDS analysis results demonstrated that AlPo was synthesized successfully without the presence of by-products.

3.2 Thermal stability and degradation mechanism of FRs

AlPi and AlPo were analyzed *via* TGA using DTG to evaluate the thermal stability and degradation mechanism of FRs as shown Fig. 4 and 5. The different degradation behavior observed results in the consequential function during the combustion process.[25] The temperature at which the weight loss of material is approximately 5 wt% is referred as the initial decomposition temperature (T_{id}) illustrated in TGA curves and the temperature at which the material exhibits the fastest weight loss is defined as the temperature of maximum mass loss rate (T_{max}).

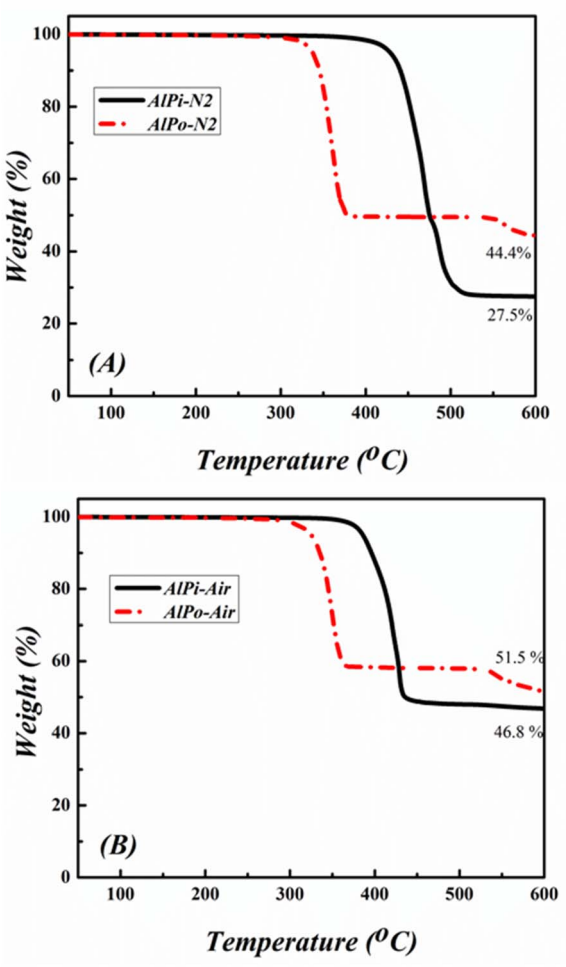

Fig. 4 TGA curves of AlPi and synthesized AlPo under nitrogen and air conditions.

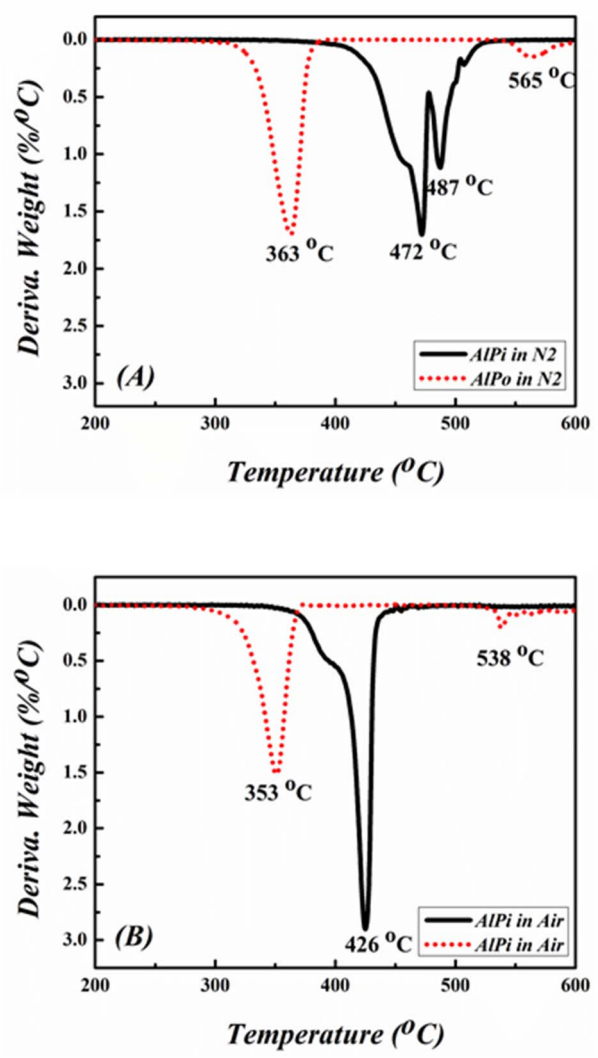

Fig. 5 DTG curves of AlPi and synthesized AlPo under nitrogen and air conditions.

The thermal degradation process depicted that AlPi decomposed in one sharp step-mass loss with 27.5 wt% and 46.8 wt% of charred residue under nitrogen and air conditions, respectively. In contrast, AlPo decomposed in *via* multiple step-mass losses with 44.4 wt% and 51.5 wt% of charred residue under nitrogen and air conditions, respectively, as shown by the TGA curves in Fig. 4. The mass of the residue of the char obtained from AlPo was higher than that of AlPi, which indicated that AlPo was effective in the condensed phase and better charring effect in flame retardancy was observed than that of AlPi. It was reported that the first step of decomposition was related to the cleavages of C–O bonding of CH_3–O and/or C–P bonding of CH_3–P and the elimination of alkyl radical $\cdot CH_3$. Subsequently, the coupling between the generated P–O–P$^{\bullet}$ and O–P–O$^{\bullet}$ radicals occurred for further network formation.[17] Additionally, the T_{id} of AlPo was lower than that of AlPi because the C–C bonding of CH_3–CH_2– in AlPi is relatively stable than that of the C–O

Table 1 UL-94 results of PA6 and PA6/FR composites

Sample	Av-t1 (s)	Av-t2 (s)	Melt dripping	Cotton ignition	UL94 rating
Pristine PA6	14	—	Yes	Yes	No rating
PA6/AlPi 15 wt%	0.75	4.5	No	No	V-0
PA6/AlPi 20 wt%	0.5	2.75	No	No	V-0
PA6/AlPo 15 wt%	0.25	18.8	No	No	V-1
PA6/AlPo 20 wt%	0.0	5.25	No	No	V-0

Table 2 Results of cone calorimetry tests for PA6 and PA6/FR composites

Sample	Pristine PA6	PA6/AlPi 15 wt%	PA6/AlPo 15 wt%
TTI (s)	48	46	35
THR (MJ m^{-2})	110	101	87
p-HRR (kW m^{-2})	959	802	394
TSP (m^2 m^{-2})	5.1	17.6	14.0
Av-EHC (MJ kg^{-1})	31.9	26.2	26.8
Residue (wt%)	−0.2	2.4	15.6

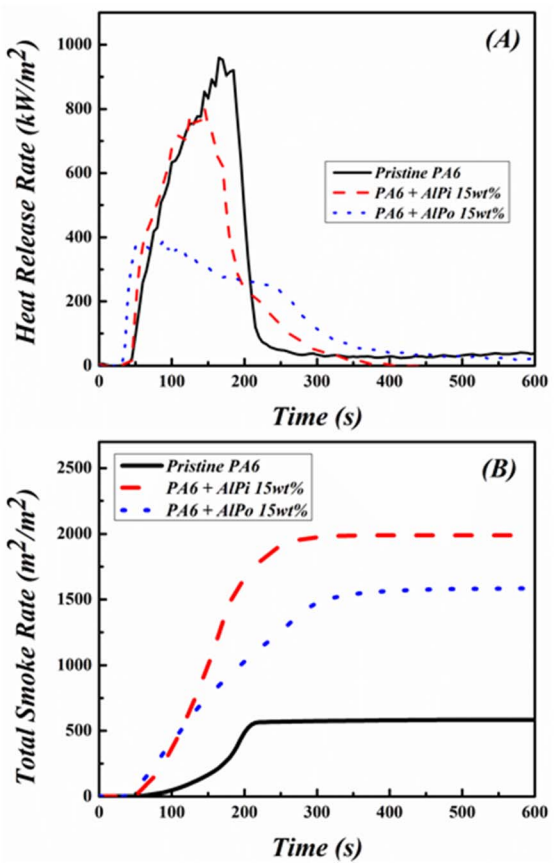

Fig. 6 Heat release rate and total smoke rate curves of pristine PA6 and PA6/FR composites.

bonding of CH_3–O– in AlPo. The T_{id} of both FRs shifted to lower temperatures under the air condition along with improvement in charred residues under the air atmosphere. This was observed because organic materials are easily oxidized and decomposed in the presence of oxygen at high temperatures. This is advantageous for extinguishing the flame and inhibiting combustion in gaseous phase. Corresponding to the TGA curves, the DTG curves of the samples were examined under nitrogen and air conditions, respectively, as shown in Fig. 5. It can be observed that the T_{max} values of AlPo was obtained at 363 °C and 353 °C under nitrogen and air atmosphere, respectively. Conversely, AlPo exhibited the T_{max} values at 472 °C and 426 °C under nitrogen and air atmosphere, respectively.

It can be concluded from these above results that AlPo is a thermally stable FR that has the ability of char formation and can generate reactive radicals which enhance flame retardancy of AlPo in gaseous phase.

3.3 Flame-retarding performance of PA6/FR composites

The UL-94 test is an indispensable method used to evaluate the flame retardancy of a polymer. In this study, the UL-94 test of PA6 and PA6/FR composites were examined and summarized in Table 1. The videos of the UL-94 test are provided in ESI S2.† During the UL-94 test, the pristine PA6 specimens exhibit dripping after ignition and an unremarkable char was formed, whereas dripping phenomenon was not observed in PA6/FR composites. In addition, the pristine PA6 specimens demonstrate that the average ignition time (av-t1) after the ignition was 14 s, wherein the specimen violently burned along with the ignited cotton and a rating was not obtained in this case. It is known that AlPi mainly works in gaseous phase, and it has been reported that V-0 rating can be achieved with the addition of 15 wt% AlPi in PA6/AlPi composite.[19] Similar results were obtained in this study as PA6/AlPi composites achieved V-0 rating from 15 wt% of loading, while PA6/AlPo composites achieved V-0 rating from 20 wt% of loading and V-1 from 15 wt% of loading. It can be explained that AlPi mainly works in gaseous phase compared with that of AlPo. Additionally, it is well-known that PA6 is a non-charrable polymer and PA6 did not exhibit charring and it decomposed to volatiles without the formation of residue during the degradation process.

3.4 Cone calorimetry test of PA6/FR composites

The cone calorimetry test was used to further analyze and compare the difference between the flame-retarding performance of AlPi and AlPo in PA6. Cone calorimetry analysis is an effective and reliable microscale method for investigating the combustion behaviors of polymer materials by directly measuring the amount of heat released from a burning sample and the corresponding amount of combustion gases released. The results of measured parameters such as time to ignition (TTI), total heat release rate (THR), peak of heat release rate (p-

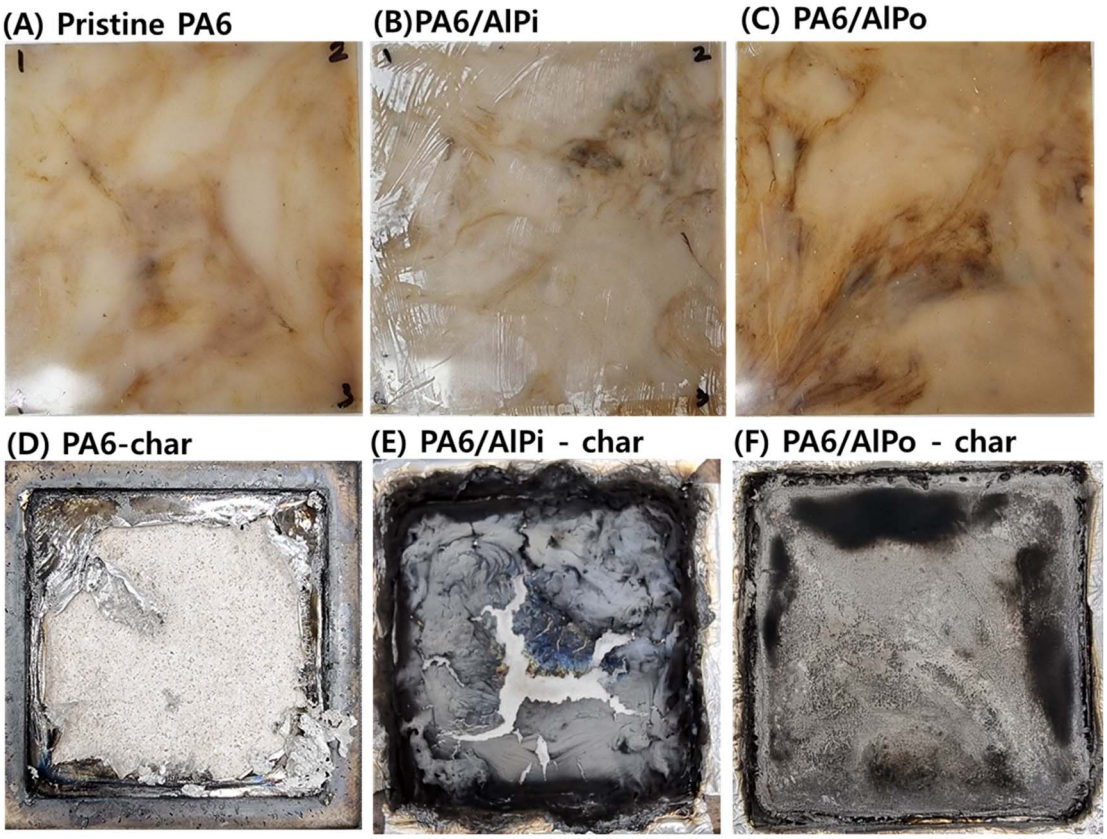

Fig. 7 Photographs of specimens before and after the cone calorimetry test.

HRR), total smoke production (TSP), average of effective heat combustion (av-EHC), and residue are listed in Table 2. The corresponding HRR and total smoke rate (TSR) curves are shown in Fig. 6. The variation of these main parameters can provide the degradation pathways of the composites.[26]

Based on the results shown in Table 2, it can be observed that the incorporation of FR in PA6 significantly decreased the p-HRR and THR values of PA6. The pHHR value of pristine PA6 decreased from 959 kW m^{-2} to 802 kW m^{-2} in PA6/AlPi composite and 394 kW m^{-2} in PA6/AlPo composite, respectively. In addition, the THR value of pristine PA6 decreased from 110 MJ m^{-2} to 101 MJ m^{-2} in PA6/AlPi composite and 87 MJ m^{-2} in PA6/AlPo composite, respectively. A low heat release value corresponds to low fire hazard. Interestingly, although AlPi achieved better flame retardancy in PA6 than that of AlPo, AlPo effectively reduced the heat generation of PA6 compared with that of AlPi. This was observed due to the char formation that protected the polymer from burning during the combustion. Therefore, the fire hazard of PA6 was significantly reduced. The charred residues of composites were considered and PA6/AlPo composite generated the highest residue at 15.6 wt%, while PA6/AlPi composite remained only 2.4 wt% of residue after cone calorimetry test. AlPo formed excessive char in the condensed phase to protect the polymer from burning and reduced heat generation and release of gases during combustion.

Conversely, the average of effective heat combustion (av-EHC) and TSP values revealed the burning degree of volatiles in the gaseous phase and the evidence of gaseous phase mechanism during the combustion, respectively. In general, the decrease in the values of EHC determines the gaseous phase effect of the flame retardant and the increase in the values of TSP was caused by the operation of FRs in the gaseous phase. Therefore, it can be concluded that AlPi works mainly in the gaseous phase when the lowest av-EHC and highest TSP values of PA6/AlPi composite were obtained at 26.2 MJ kg^{-1} and 17.6 m^2 m^{-2}, respectively. Meanwhile, the av-EHC value decreased from 31.9 MJ kg^{-1} of pristine PA6 to 26.8 MJ kg^{-1} of PA6/AlPo composite and the TSP value increased from 5.1 m^2 m^{-2} of pristine PA6 to 14.0 m^2 m^{-2} of PA6/AlPo composite. The reduction in the av-EHC and increase in the TSP after the addition of AlPo in PA6 verified that AlPo operated well in gaseous phase and AlPo can effectively work in dual phase (gaseous and condensed phases). Despite the increase of TSP values was observed in PA6/FR composites, PA6/AlPo composite generated less smoke than PA6/AlPi composite.

Furthermore, the digital photos of specimens before and after the cone calorimetry test are illustrated in Fig. 7. It can be observed that charred residue was absent on the surface of the pristine PA6 which indicated that PA6 was completely decomposed. In contrast, the obtained residue compactly and continuously covered the hole surface for PA6/AlPo composite, while PA6/AlPi composite produced thin and broken char residue in comparison with that of PA6/AlPo composite. In addition, the photos of cross section illustrated in ESI S3† assisted the discussion related to the charring effect. It can be stated that AlPi mainly worked in the gaseous phase, while AlPo worked in gaseous and condensed phases.

3.5 Thermal stability of PA6/FR composites

TGA combined with DTG is an effective technique that can be used to analyze the thermal behaviors of materials and thermal degradation of FRs in PA. Fig. 8 shows the TGA and DTG curves of PA6 and PA6/FRs composites under nitrogen atmosphere. The related data including $T_{5\%}$, T_{max}, and residue at 700 °C are presented in Table 3. Theoretical residue based on experimental residue of individual FR weighted by the mass percentage of FR in the formulation and is used to assist the discussion about reaction between FR and PA6 after the decomposition.

As we mentioned that PA6 is a non-charrable polymer, TGA curve of PA6 shows that PA6 decomposed completely in one sharp step. The above results demonstrated that AlPi had higher values of T_{id} and T_{max} than that of AlPo and similar results were observed for PA6/FR composites as shown in Fig. 8. The T_{id} and T_{max} of PA6/FR composites shift to lower values when comparing with pristine PA6, which indicated that the addition of FR in PA6 decreased the initial thermal stability of the composite. From detailed values in Table 3, pristine PA6 exhibited $T_{5\%}$ and T_{max}

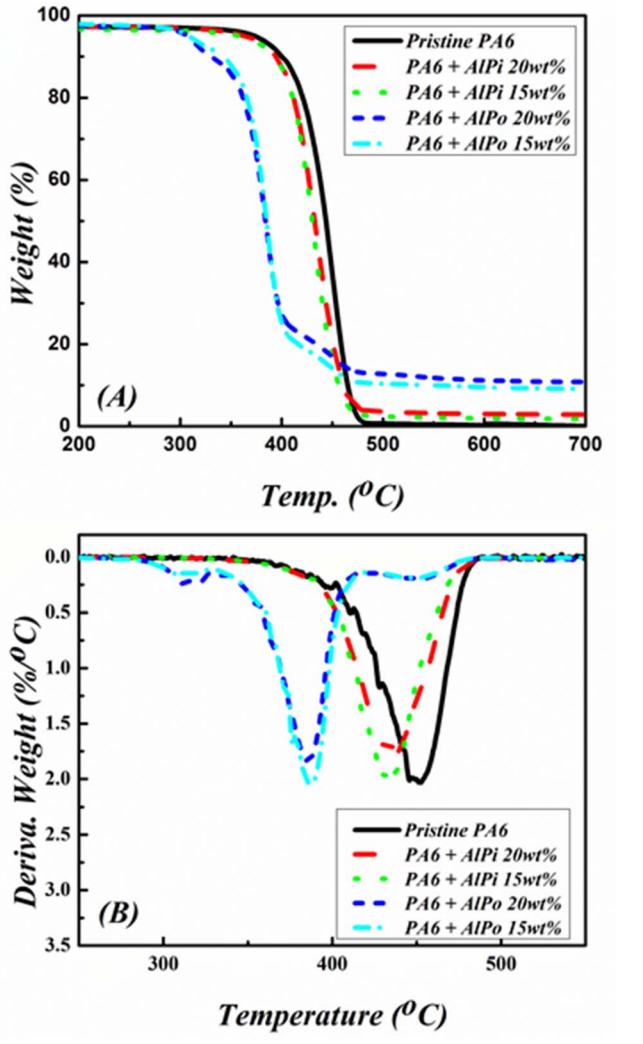

Fig. 8 TGA and DTG curves of PA6 and PA6/FR composites measured under nitrogen atmosphere.

Table 3 TGA results of PA6 and PA6/FR composites under nitrogen atmosphere

Sample	$T_{5\%}$ (°C)	T_{max} (°C)	Theoretical residue at 700 °C[a] (wt%)	Residue at 700 °C (wt%)
Pristine PA6	374	456	0.05	0.05
PA6/AlPi 15 wt%	358	434	4.17	1.76 (↓)
PA6/AlPi 20 wt%	364	438	5.54	2.83 (↓)
PA6/AlPo 15 wt%	308	387	6.66	9.01 (↑)
PA6/AlPo 20 wt%	307	385	9.22	10.81 (↑)

[a] Theoretical residue based on experimental residue of individual FR weighted by the mass percentage of FR in the formulation.

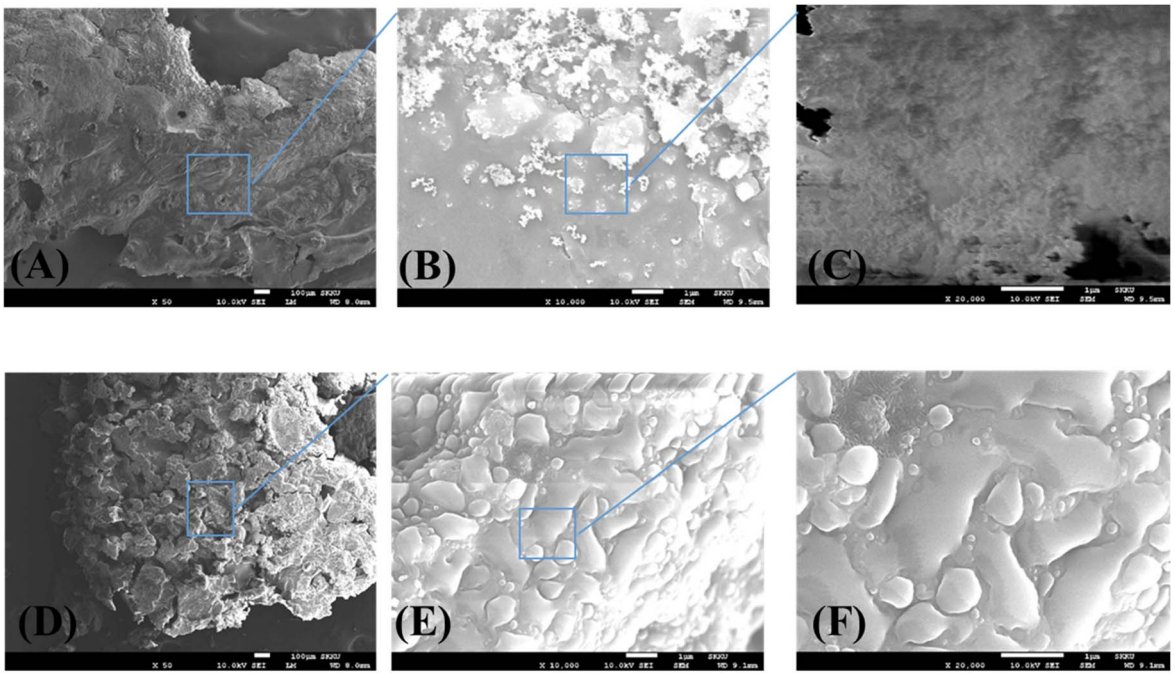

Fig. 9 FE-SEM images of composite surfaces after UL-94 test. (A–C): Charred residue of PA6/AlPi composite. (D–F): Charred residue of PA6/AlPo composite.

values of 374 °C and 456 °C, respectively. The PA6/AlPi composite with 15 wt% of AlPi loading exhibited $T_{5\%}$ and T_{max} values of 358 °C and 434 °C, respectively. The PA6/AlPo composites with 15 wt% of AlPo loading exhibited $T_{5\%}$ and T_{max} values of 308 °C and 387 °C, respectively.

A comparison between the experimental char residues with that of the calculated char residues demonstrated that PA6/AiPi composites generated lower char yields, whereas PA6/AlPo composites formed higher amount of char residues. This indicated that AlPo caused the charring effect by significantly contributing to the carbonization during ignition, whereas AlPi predominantly decomposed to form volatile products without improving the char formation of PA6.

3.6 Charred residue analysis

The microstructure of the external surface of the char residue after the UL-94 test was investigated to further analyze the flame retardancy of FR in PA6 as shown in Fig. 9. Fig. 9A–C depict that in the case of AlPi, the external surface of char was covered with

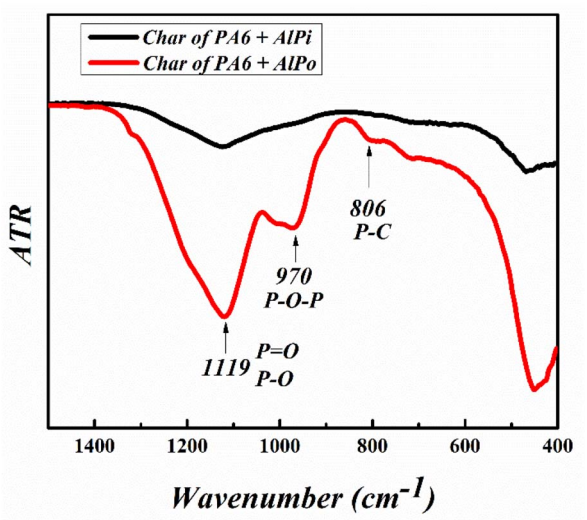

Fig. 10 ATR analysis of residues after cone calorimeter.

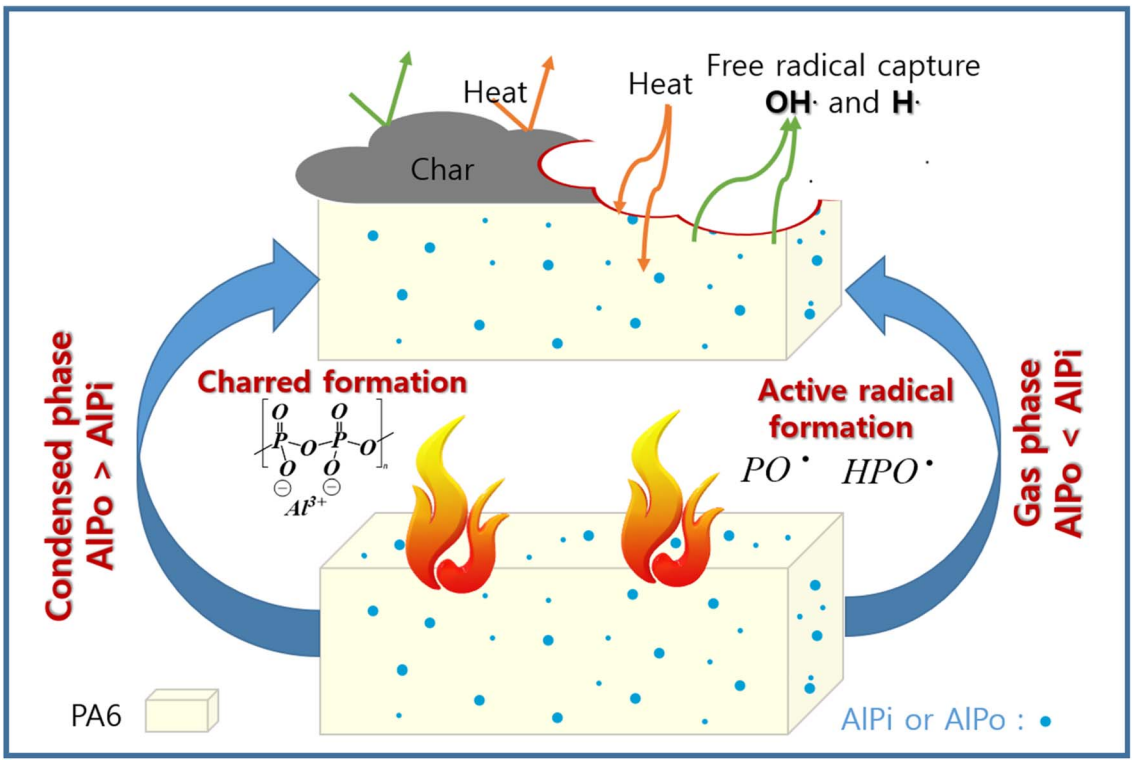

Fig. 11 Schematic diagram of the proposed flame-retarding mechanism model of PA6/FRs.

porous bubbles which indicated that AlPi did not promote the carbonization of PA6 during fire extinguishing. The fundamental reason of that is mainly working at gas phase of AlPi with free radical quenching in flame retardancy[27,28] Fig. 9D–F depict that the external surface of PA6/AlPo composite char exhibited a compact dense structure without cracks or bubbles which can act as shielding to insulate the heat and gas. Therefore, it can be concluded that AlPo promoted char formation of PA6 during ignition and effectively protected PA6 from heat penetration compared with that of AlPi.

The charred residues of PA6/FRs after cone calorimetry were analyzed *via* ATR to evaluate the thermal degradation mechanism of FRs, and the result is presented in Fig. 10. The appearance of a strong band at 970 cm^{-1} of PA6/AlPo char was attributed to the P–O–P stretching vibration. Additionally, the P–O/P═O vibrations observed at 1044 cm^{-1}/1168 cm^{-1} became broader, while weaker adsorption was observed for the PA6/AlPi char. Therefore, it can be concluded that the flame retardancies of AlPo were based on the formation of a stable P–O–P based network in the condensed phase to effectively inhibit the combustion compared with that of AlPi.

The difference between the potential flame retardancy mechanisms of AlPi and AlPo in PA6 is shown in Fig. 11. In the gaseous phase mode of action, AlPi exhibited better performance than that of AlPo because the P–C bonding produced active phosphorus containing radicals, which capture the free radicals of the material generated by combustion. Meanwhile, AlPo formed char and effectively performed in the condensed phase compared with that of AlPi. Although AlPi exhibited the charring effect, it is not unstable and weak. The P–O bonding formed –P–O–P crosslinking networks to improve the thermal stability and protect the polymer surface from heat and oxygen penetration. Therefore, this study aids the development of suitable FRs required for future investigation.

4. Conclusions

In this study, an aluminum methyl methoxyphosphonate (AlPo)-based FR was synthesized. The thermal stability of AlPo and its flame retardancy in polyamide 6 was evaluated. The thermal stability and flame retardancy of AlPo were compared with that of aluminum diethylphosphinate (AlPi)-based FR. AlPi with phosphinate structure consisting of multiple P–C bonds in the molecule which aided the gas-generating mechanism and effectively worked for PA6. However, it generated excessive heat and emissions. Meanwhile, AlPo consisted of P–C and P–O bonds in the molecular structure. Therefore, it operated in gaseous and solid phases, and it generated a significant amount of char to protect the PA6 surface from heat and oxygen exposure during the burning process. In addition, AlPo is a potential FR due to the combination of both phases and it fulfills the requirements for good fire resistance for PA6 resins and reduces the amount of heat and gas generated during the combustion process.

Author contributions

Hai Vothi: writing – original draft, investigation, methodology, supervision. Chowon Kim: formal analysis. TanBinh Nguyen:

formal analysis, writing – editing. Jinwoo Lee: writing – editing. Lan-Anh T. Nguyen: formal analysis. Jonghwan Suhr: funding acquisition, supervision.

Conflicts of interest

There are no conflicts to declare.

Acknowledgements

This work was supported by the Center for Composite Materials & Concurrent Design, Research & Business Foundation. We would like to thank Editage (**https://www.editage.co.kr**) for english language editing.

References

1 *Encyclopedia of Physical Science and Technology*, ed. R. A. Meyers, Elsevier B.V., 3rd edn, 2001.
2 *Encyclopedia of Electrochemical Power Sources*, ed. Jürgen Garche, Elsevier B.V., 2009.
3 A. R. Jha, *Next-Generation Batteries and Fuel Cells for Commercial, Military and Space Applications*, 2012.
4 T. S. Ghanta, S. Aparna, N. Verma and D. Purnima, *Polym. Eng. Sci.*, 2020, **60**, 1717–1759.
5 M. Coquelle, S. Duquesne, M. Casetta, J. Sun, S. Zhang and S. Bourbigot, *Polym. Degrad. Stab.*, 2014, **106**, 150–157.
6 E. Braun and B. C. Levin, *Fire Mater.*, 1987, **11**, 71–88.
7 C.-H. Choi, J.-M. Cho, Y. Kil and Y. Yoon, *Development of Polymer Composite Battery Pack Case for an Electric Vehicle*, 2013.
8 S. V Levchik and E. D. Weil, *Polym. Int.*, 2000, **49**, 1033–1073.
9 E. S. Gonçalves, L. Poulsen and P. R. Ogilby, *Polym. Degrad. Stab.*, 2007, **92**, 1977–1985.
10 C. K. Kundu, Z. Li, L. Song and Y. Hu, *Eur. Polym. J.*, 2020, **137**, 109911.
11 S. Wendels, T. Chavez, M. Bonnet, K. A. Salmeia and S. Gaan, *Materials*, 2017, **10**(7), 784.
12 H. Vothi, C. Nguyen, K. Lee and J. Kim, *Polym. Degrad. Stab.*, 2010, **95**, 1092–1098.
13 R. Nazir and S. Gaan, *J. Appl. Polym. Sci.*, 2020, **137**, 218–244.
14 H. Vahabi, F. Laoutid, M. Mehrpouya, M. R. Saeb and P. Dubois, *Mater. Sci. Eng., R*, 2021, **144**, 100604.
15 S. Rabe, Y. Chuenban and B. Schartel, *Materials*, 2017, **10**(5), 455.
16 N. Levinţa, Z. Vuluga, M. Teodorescu and M. C. Corobea, *SN Appl. Sci.*, 2019, **1**, 422.
17 H. Vothi, C. Nguyen, L. H. Pham, J. Kim and D. Q. Hoang, *Polym. Bull.*, 2021, **78**, 6761–6776.
18 H. Ge, G. Tang, W.-Z. Hu, B.-B. Wang, Y. Pan, L. Song and Y. Hu, *J. Hazard. Mater.*, 2015, **294**, 186–194.
19 U. Braun, H. Bahr and B. Schartel, *e-Polymers*, 2010, 041.
20 F. Tomiak, A. Schoeffel, K. Rathberger and D. Drummer, *Polymers*, 2021, **13**, 2712.
21 H. Vothi, C. Nguyen, D. Q. Hoang and J. Kim, *Polym. Bull.*, 2020, **77**, 1503–1518.
22 W. Huang, W. He, L. Long, W. Yan, M. He, S. Qin and J. Yu, *Polym. Degrad. Stab.*, 2018, **148**, 26–41.
23 H. Feng, D. Li, B. Cheng, T. Song and R. Yang, *J. Hazard. Mater.*, 2022, **424**, 127420.
24 B. Liu, J. Xu, H. Xue, Z. Shu, G. Xu, H. Ou and Y. Weng, *J. Appl. Polym. Sci.*, 2021, **138**(19), 1–11.
25 W. Tao, X. Hu, J. Sun, L. Qian and J. Li, *Polym. Degrad. Stab.*, 2020, 109092.
26 H. Feng, Y. Qiu, L. Qian, Y. Chen, B. Xu and F. Xin, *Polymers*, 2019, **11**, 74.
27 L. Shao, B. Xu, W. Ma, J. Wang, Y. Liu and L. Qian, *J. Appl. Polym. Sci.*, 2020, **137**, 48699.
28 Y. Cao, L. Qian, Y. Chen and Z. Wang, *J. Appl. Polym. Sci.*, 2017, **134**, 45126.